Nano World Journal

https://doi.org/10.17756/nwj.2023-127

Research Article

Open Access

Iron Oxide Nanoparticles Synthesized Using Mentha piperita Extract and Evaluation of Its Antibacterial and Antimigratory Potential on Highly Metastatic Human Breast Cells

Huzaifa Umar[1*], Maryam Rabiu Aliyu[2] and Dilber Uzun Ozsahin[1,3,4]

[1]*Operational Research Center in Healthcare, Near East University, TRNC Mersin 10, Nicosia, Turkey*
[2]*Department of Energy System Engineering Cyprus International University, Nicosia, Northern Cyprus via Mersin 10, Turkey*
[3]*Department of Medical Diagnostic Imaging, College of Health Sciences, University of Sharjah, Sharjah, United Arab Emirates*
[4]*Research Institute for Medical and Health Sciences, University of Sharjah, Sharjah, United Arab Emirates*

[*]Correspondence to:
Huzaifa Umar
Operational Research Center in Healthcare,
Near East University,
TRNC Mersin 10,
Nicosia, Turkey.
E-mail: Huzaifa.umar@neu.edu.tr

Received: November 03, 2023
Accepted: November 30, 2023
Published: December 05, 2023

Citation: Umar H, Aliyu MR, Ozsahin DU. 2023. Iron Oxide Nanoparticles Synthesized Using *Mentha piperita* Extract and Evaluation of Its Antibacterial and Antimigratory Potential on Highly Metastatic Human Breast Cells. *NanoWorld J* 9(4): 144-151.

Published by United Scientific Group

Abstract

Iron oxide nanoparticles (Fe_2O_3 NPs) stabilized with *Mentha piperita* obtained from Cyprus were synthesized. The study focused on exploring the anti-migratory potential, cytotoxicity, anti-proliferative and antimicrobial potential of Fe_2O_3 NPs using wound healing assay, trypan blue, 3-[4,5-dimethylthiazol-2-yl]-2,5-diphenyltetrazolium bromide (MTT) and disc diffusion, respectively. Fourier-transform infrared spectroscopy (FTIR), X-ray diffraction (XRD), Ultraviolet-Visible spectroscopy (UV-vis), scanning electron microscopy (SEM), and energy-dispersive X-ray spectroscopy (EDX) were used to characterize the Fe_2O_3 NPs. The spectra obtained from FTIR, XRD, and SEM-EDX confirmed the formation of Fe_2O_3 NPs. The analysis of UV-Vis spectra indicates an absorption peak at 302 nm, thereby confirming both the successful synthesis and remarkable stability of the NPs. The NPs exhibited uniform spherical morphology and contained Fe, O, and N, indicating the synthesis of Fe_2O_3 NPs. Additionally, the Fe_2O_3 NPs formed through biosynthesis demonstrated antimicrobial capabilities against *Escherichia coli* and *Bacillus cereus*. The significant anti-migratory potential on MDA-MB 231 human breast cancer cells was observed with lower concentrations of the biosynthesized Fe_2O_3 NPs, and higher concentrations revealed cytotoxic effects on the cells with an IC_{50} of 95.7 µg/ml. Stable Fe_2O_3 NPs were synthesized using *M. piperita* aqueous extract, and it revealed antimicrobial activity on *E. coli* and *B. cereus*, cytotoxic, anti-proliferative and anti-migratory effect on highly metastatic human breast cancer cell lines.

Keywords

Anti-proliferative, Cytotoxicity, Stabilizing agent, UV-Vis spectroscopy, Trypan blue

Introduction

Nanomaterials have caught the attention of medical researchers due to their advantageous properties. These materials have a similar size to biological molecules such as enzymes, proteins, and lipids, which allows for more effective interactions. When compared to typical drugs, nanomaterials are smaller in size, with wide surface area, and unique magnetic, physicochemical, catalytic, and mechanical properties, and can also accumulate more efficiently in targeted organs, ultimately enhancing their effectiveness [1]. The NPs have proven to be valuable for bridging materials from large to atomic scale. Various precursors such as iron, nickel, zinc, copper, silver, and gold nanoparticles are commonly utilized in their synthesis due to their favorable properties and a broad range of applications [2-4]. The use of eco-friendly methods in nanotechnology is rapidly expanding,

creating non-toxic and stable metal oxide NPs. These particles possess unique physical and chemical properties, making them compatible with the human body and useful for various purposes, including cancer treatment, drug delivery, medical imaging, diabetes treatment, biosensors, antimicrobial agents, and cosmetics [5].

Iron oxide, in its hematite (α-Fe_2O_3) form, is a thermodynamically stable substance that exhibits n-type semiconductor properties [6]. Hematite iron oxide (α-Fe_2O_3) exhibits a core and shell structure, giving them both hydrous iron oxides and metallic iron [7]. By utilizing controlled precipitation methods that involve inorganic metal salts or washing the material, Hematite nanoparticles (α-Fe_2O_3 NPs) can be effectively synthesized. The size of these nanostructures can also be adjusted through calcination. It is important to note that the synthetic method adopted greatly influences the quality of the NPs. Therefore, by improving the synthetic method used, we can significantly enhance the quality of the NPs [8]. The therapeutic properties of Fe_2O_3 NPs have been extensively studied because of their biocompatibility. They are highly favored among researchers due to their potential to treat diverse medical conditions [1]. Several ways to treat cancer include using Fe_2O_3 NPs to generate reactive oxygen species or localized heat or combining Fe_2O_3 NPs with a chemotherapeutic drug such as paclitaxel (Fe_2O_3 NPs-PAX). Studies have shown that Fe_2O_3 NPs-PAX are more effective in destroying prostate tumor cells *in vitro* on PC3 and CWR22R human prostate cancer cells and *in vivo* on C4-2-cell-derived xenograft tumours in athymic nude mice. Similarly, Fe_2O_3 NPs associated with cisplatin have demonstrated more significant cytotoxicity towards A549 cells as compared to free cisplatin [9, 10]. Costly and hazardous physical and chemical techniques are involved in producing metal oxide NPs, often utilizing antagonistic chemicals as stabilizers [11].

Integration of biosynthesis, green chemistry, nanoscience, and technology has created a network of interconnected fields to eliminate the hazardous effect of the synthesized NPs through chemical means. This approach to eco-friendliness is not only cost-effective and safe, but it is also a preferred method over other techniques [12]. Developing metallic oxide nanomaterials, such as Fe_2O_3 NPs, via green route is an advancement in this field of biomedical research [13]. Iron oxide is essential in the biomedical field for diagnostic, therapeutic, drug delivery, and bioremediation purposes. The synthesis of NPs is a significant concern because biological methods are eco-friendly, while chemical methods are considered toxic [14]. Plants are often perceived as a convenient and accessible means of producing various types of NPs. They are easy to handle, have no major risks, and are cost-effective, making them an attractive option for many people [15]. Plant extracts contain bioactive compounds that offer numerous health benefits. These compounds also act as capping and reducing agents during synthesis, preventing agglomeration, and providing crucial stability to the resulting NPs [16].

M. piperita, also known as peppermint, is a strongly scented herb that belongs to the Lamiaceae family and is perennial and glabrous. For over a millennium, this particular species has been grown in temperate and subtropical regions [17, 18]. It is commercially valuable and has a distinct aroma (mints) that is used in pharmaceuticals, herbal formulations, food industries and cosmetics, which is why it is cultivated in temperate regions of Europe, the United States, Asia, and Mediterranean countries [19, 20]. *M. piperita* is a nutritious leafy vegetable that is rich in vitamins and minerals. It is commonly used as a flavoring agent in various food items, beverages, chewing gums, and candies [21, 22]. Mint contains volatile components such as menthol, menthone, menthyl acetate, menthofuran, and 1,8-cineol. Additionally, it also contains non-volatile components like flavonoids, phenolic acids, amino acids, nucleosides, and terpenoids, which are the primary active components of mint responsible for its therapeutic potential [22-24]. Plant compounds such as flavonoids, phenols, and terpenoids are predominantly found in the leaves, while diterpenes are present in the leaves and stems [25]. In addition, the dried leaves of *M. piperita* contained essential mineral nutrients like potassium, calcium, sodium, phosphorus, zinc, and magnesium [26].

Our study highlights the successful synthesis of stable Fe_2O_3 NPs using *M. piperita* aqueous extract. Spectroscopic and microscopic methods were utilized to characterize the synthesized NPs. Our evaluation of the Fe_2O_3 NPs revealed their anti-migratory, anti-proliferative, and cytotoxic potential on MDA-MB 231 cells using wound heal, MTT, and trypan blue assays. In addition, the antimicrobial potential of the Fe_2O_3 NPs was studied against *E. coli* and *B. cereus* using standard methods.

Materials and Methods

Materials

Fresh flowers of *M. piperita* were collected from a farm in Lefkosa (Lat.34° and 36° N; Long 32° and 35° E) in November 2021, the Turkish Republic of Northern Cyprus and authenticated at the Botany Department of Cyprus International University, and a voucher number of CIU/BOT/0012 was given to the specimen and kept at the herbarium of the institute. All the aqueous solutions were prepared using triple distilled de-ionized water.

All chemicals and reagents used throughout the experiment are of analytical grades. The chemicals used include: Iron (III) chloride ($FeCl_3$) (Merc), Dimethyl Sulfoxide (DMSO) (Sigma-Aldarich Inc.), Dulbecco's Modified Eagle Medium (DMEM) (Gibco by Life Technologie, USA), Fetal Bovine Serum (FBS) (Gibco by Life Technologies, USA), Glycine (Sigma-Aldarich Inc.), 0.25% Trypsin and 0.4 % Tryphan Blue (Gibco by Life Technologies, USA), L-Glutamine 200 mm (Gibco by Life Technologies, USA), Distilled Water (Gibco by Life Technologies, USA), 70% Ethanol (Merck), and Penicillin (Gibco by Life Technologies, USA).

Biosynthesis of Fe2O3 NPs

The Fe_2O_3 NPs synthesis with *M. piperita* was achieved using the method employed by Yusefi et al. with slight modification [27]. Fresh leaves of *M. piperita* were collected, weighed, dried, pulverized to powder and extracted in aqueous medium in an Erlenmeyer flask. Biosynthesis of Fe_2O_3 NPs was carried

out using 0.001 M $FeCl_3$ solution and 20% *M. piperita* aqueous extract. After being centrifuged at 10,000 rpm for 30 min, the mixture underwent 2 to 3 washes with Millipore water to eliminate impurities and was kept at 180 °C for five consecutive hours.

Characterization of Fe2O3 NPs

The analysis of Fe_2O_3 NPs using UV-Vis spectroscopy was conducted using a Shimadzu UV-2450 instrument, in which the NPs were dissolved in deionized water and thoroughly mixed with a sonicator. The resulting solution was then filtered and placed in a 10 mm cuvette, where the spectrum was measured across the wavelength range of 200 to 900 nm at room temperature. Furthermore, functional groups in the Fe_2O_3 NPs were identified by employing a FTIR operating at a frequency range of 500 to 4000cm^{-1}. The crystalline nature of the Fe_2O_3 NPs was assessed using the Rigaku ZSX Primus II X-ray diffractometer (XRD). This involved using powdered samples in the X-ray diffractometer, equipped with CuK radiation, to examine the structural characteristics of the NPs. Additionally, the morphological structure of the NPs was examined using a SEM, and elemental mapping was conducted through EDX.

Determination of antimicrobial activity

Antimicrobial activity of Fe_2O_3 NPs on *B. cereus* (ATCC 9634) and *E. coli* (O157:H7) was carried out on Muller-Hinton agar [28]. After treating the organisms with Fe_2O_3 NPs and letting them incubate overnight, inhibition zones were evaluated following standard microbiology-based protocols by NCCLS (National Committee for Clinical Laboratory Standards) recommended by World Health Organization.

Cytotoxicity, proliferation, and anti-migratory assay

The effect of the synthesized Fe_2O_3 NPs on MDA-MB 231 cells were assessed by employing a modified procedure based on the method described by Umar et al. [29]. These cells were subjected to varying concentrations of the extract, specifically 500, 250, 50, and 10 µg/ml, for a period of 24 h. Following removing the treatment, diluted trypan blue was introduced and incubated it for 10 min in darkness. Subsequently, the number of both dead and viable cells were counted.

Cell proliferation after exposure to various Fe_2O_3 NPs concentrations was evaluated in MDA-MB 231 cells using the methodology detailed in Umar et al. with slight modification [5]. Specifically, cells were treated with Fe_2O_3 NPs at 500, 250, 50, and 10 µg/ml concentrations, with an initial cell count of 3 x 10^4. Following removal of the culture medium, 600 µl growth media was introduced, and 5 mg/ml of MTT was added to the cells. After the incubation period, the MTT solution was aspirated, and a mixture of DMSO (890 µl) and glycine buffer (110 µl) was added. Additionally, absorbance was measured at 570 nm using an Absorbance Microplate Reader (ELX 800TM). Multiple measurements were conducted.

The anti-migration ability of Fe_2O_3 NPs was studied on MDA-MB 231 cells, following some methods with slight modifications [30]. Cells were cultured in 35 mm dishes, and lines were drawn on the dishes to create scratch wounds. MDA-MB 231 cells were plated at 1 x 10^6/ml and 5 x 10^5/ml per dish; pipette tips were used to create three scratch lines, treated with 50 and 10 µg/ml and incubated for 24 h. Captured images of the initial and subsequent wounds using a camera attached to an inverted microscope at x100 magnification. Image processing software (ImageJ) was used to analyze the recovery wound area and calculate cell migration using equation 1.

$$\text{Mo I} = 1 - \left(\frac{W_t}{W_0} \right) \quad (1)$$

Where, Mo I, motility index; W_t, the width of the wound at 24 h; and W_0, initial wound width at 0 h.

Statistical data analysis

Our experimental results using averages and associated standard deviations were displayed and carefully examined the data using IBM SPSS Statistics version 21 and employed a one-way ANOVA and Student's t-test where applicable. The experiments were conducted in triplicates, each time maintaining a sample size of at least n ≥ 3. P-values below 0.05 as indicative of statistical significance were considered.

Results and Discussion

Characterization

In this study, Fe_2O_3 NPs were synthesized using *M. piperita* extract as a stabilizing agent. The synthesis was rapid due to the phytoconstituents in the plant extract that serve as reducing agents.

UV-Vis spectra analysis was used to validate the formation of Fe_2O_3 NPs a few hours after the reaction and as a result of color shift (from greenish to reddish brown). The UV-Vis validation revealed an absorption peak at 302 nm, which can be attributed to the surface plasmon resonance effect due to the formation of Fe_2O_3 NPs, as shown in figure 1. Our absorption peak is within the range at which Fe_2O_3 NPs are absorbed because studies revealed that Fe_2O_3 NPs appear at an absorption peak rate of 295 - 305 nm [31].

The Fe_2O_3 NPs functional group was determined by analyzing their FTIR spectra within a range of 400 to 4500 cm^{-1},

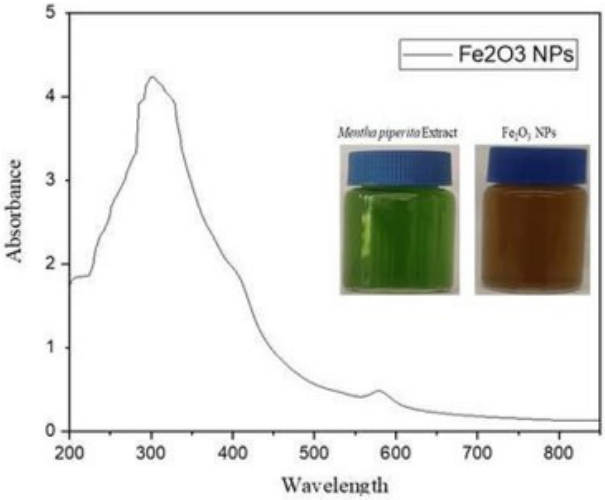

Figure 1: UV-Vis spectrum of the synthesized Fe_2O_3 NPs.

as presented in figure 2. The peaks indicated the stretching vibration of Fe-O and Fe-O-H stretching observed at 764 cm^{-1} and 618 cm^{-1}, respectively [32]. The participation of the plant extract in the synthesis of Fe_2O_3 NPs was indicated by the stretching of aliphatic and aromatic N-O amine oxide stretch bands at 841 cm^{-1} and 1066 cm^{-1}, respectively [32]. Additionally, firm peaks at 1971 cm^{-1} and 2156 cm^{-1} were associated with the O-H stretching vibration of surface-adsorbed water molecules [33]. Stabilizing and capping of NPs are achieved due to the participation of phytochemicals such as flavonoids and phenols [2].

The phase purity of the Fe_2O_3 NPs synthesized using *M. piperita* was ascertained using XRD, as shown in figure 3. The prominent peaks observed from our XRD analysis at 012, 104, 110, 113, 202, 024, 116, 018, 214, 300, 208, 1010 and 220 correspond to 2θ values of 24.05°, 33.01°, 35.53°, 40.74°, 49.31°, 53.87°, 57.41°, 62.27°, 63.85°, 71.69°, 75.32°, and 80.5°, respectively. The crystalline nature of our synthesized Fe_2O_3 NPs was confirmed, following the presence of the peaks mentioned recently and is in conformity with many studies [34]. The XRD pattern revealed from our synthesized Fe_2O_3 NPs results from reduced metal oxide ions by *M. piperita* extract, and an average crystal size of 26 nm was calculated using equation 2.

$$Crystal\ size(D) = \frac{k\lambda}{(\beta \cos\theta)} \quad (2)$$

From equation 2, λ represents the shape factor, β is the total width half maximum in radians, and θ is the Bragg's angle in radians for Cu-Kα radiation.

The synthesized Fe_2O_3 NPs were examined using SEM to determine their morphology and chemical composition. The results showed that the Fe_2O_3 NPs had an irregular spherical shape without agglomeration (Figure 4). This could be due to phytochemicals present in the *M. piperita* extract. Although there was a variability in the size, the average size of the NPs from the SEM image was between 21 - 26 nm. The surface morphology of the NPs plays a significant role in understanding their role, and the involvement of plant extract in reducing their size has been previously reported [35].

Additionally, the chemical composition of the Fe_2O_3 NPs was revealed by the EDX spectra present. The result revealed that the NPs contained a high percentage of Fe and O, with small amounts of N and Ca also present (Figure 5). This confirmed the participation of the *M. piperita* extract in the formation of the NPs. Furthermore, an elemental mapping showed that Fe and O were distributed in the NPs at 76.23% and 27.40%, respectively.

Antimicrobial activity

The effectiveness of synthesized Fe_2O_3 NPs against *B. cereus* and *E. coli* was ascertained and compared to *M. piperita*, and ciprofloxacin (control group). Our result revealed good antimicrobial potential on the bacteria, and our synthesized Fe_2O_3 NPs revealed significant antimicrobial effects on both *B. cereus* and *E. coli*. When compared with *M. piperita* aqueous extract similar ($p < 0.0001$; Figure 6a). In addition, significant difference was also observed when compared with ciprofloxacin treated group ($p < 0.0001$; Figure 6a). The antibacterial

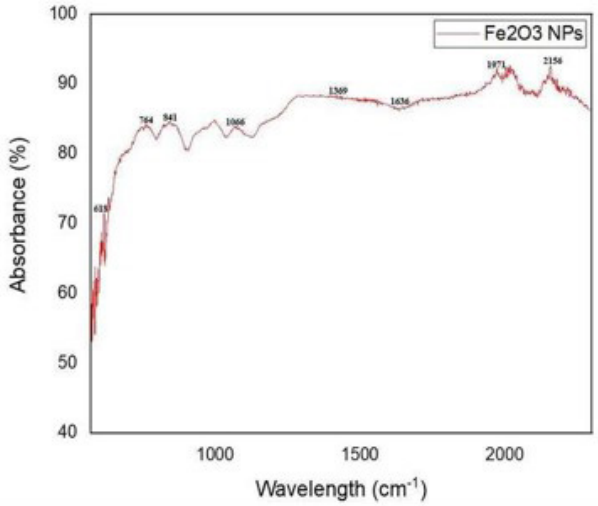

Figure 2: FTIR spectra of the synthesized Fe_2O_3-NPs.

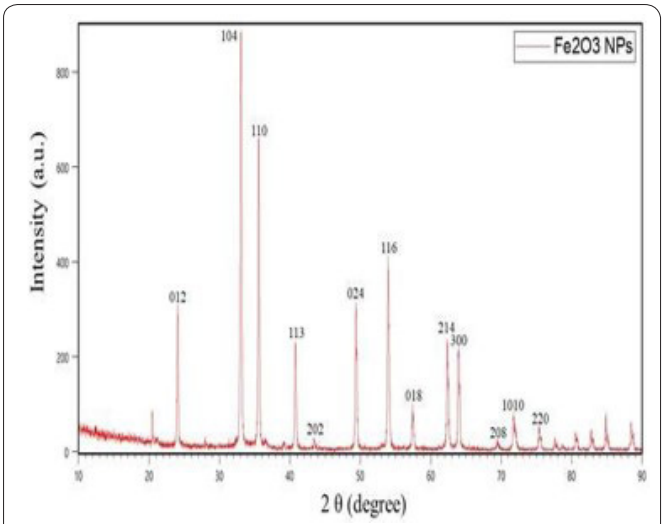

Figure 3: XRD image of the synthesized Fe_2O_3 NPs.

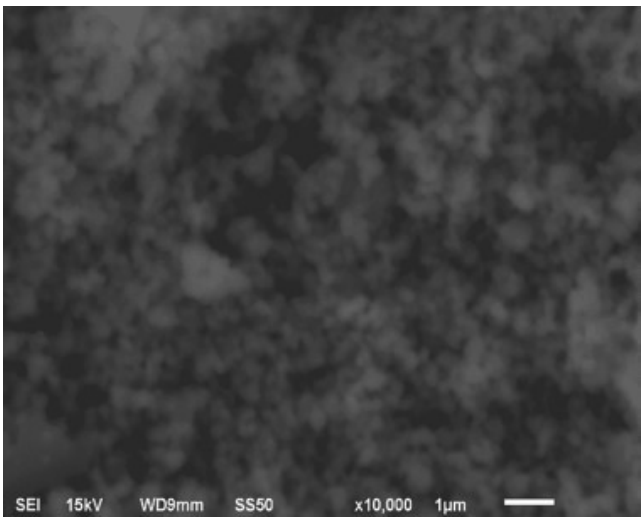

Figure 4: SEM image of the synthesized Fe_2O_3 NPs.

potential revealed by our NPs against both bacteria might be as a result of metallic irons present in the NPs, less effect was seen in those treated with the plant extract. Our findings align with numerous studies, demonstrating the potential of Fe_2O_3

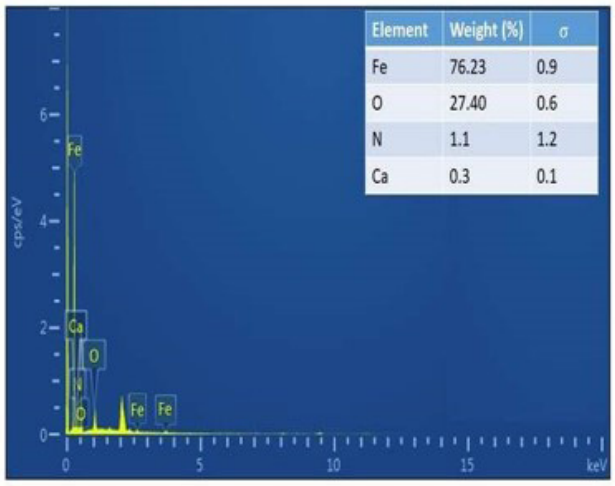

Figure 5: EDX of the synthesized Fe_2O_3 NPs.

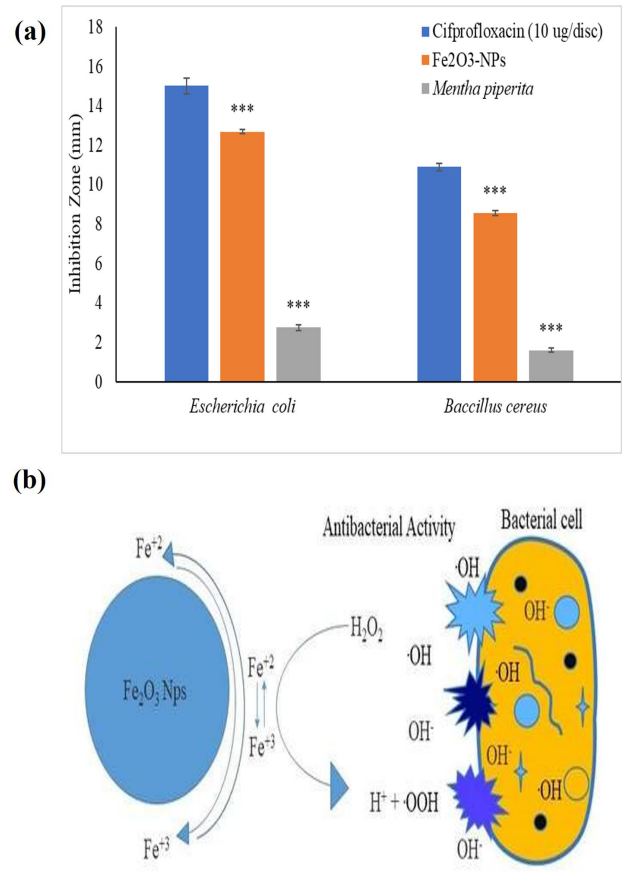

Figure 6: (a) Antimicrobial potential of Fe_2O_3 NPs compared with *M. piperita* extract, *M. piperita* extract, and ciprofloxacin. **(b)** Predicted mechanism against the antimicrobial activity of synthesized Fe_2O_3 NPs using *M. piperita* extract. ***P<0.0001.

NPs synthesized using biological means against *E. coli*, *B. Cereus*, *Staphylococcus aureus*, and *Pseudomonas aeruginosa* [36-39]. Irshad et al. revealed the antibacterial activity of synthesized Fe_2O_3 NPs using *Punica granatum* peel extract against various microorganisms [40], and their findings follow our results. According to our research, the microbial potential can be attributed to the release of metallic ions by NPs, as shown in figure 6b. These ions attach to the bacterial cell wall through electrostatic interaction, targeting thiol functional groups. The Fe_2O_3 NPs can then penetrate the cell wall, enabling the entry of nutrients. This process ultimately leads to decreased protein levels and cell death, as illustrated in the accompanying predicted mechanism diagram (Figure 6b).

Cytotoxic, anti-proliferative, and anti-migratory potentials

The effect of various concentrations (0 to 500 µg/ml) of Fe_2O_3 NPs on MDA-MB 231 following 24 h incubation period, the effect on the cytotoxicity and proliferation were determined using trypan blue assay and MTT, respectively (Figure 7a and 7c). Light microscopy images of the cells treated with various concentrations of Fe_2O_3 NPs are also shown in figure 7b and 7d. The Fe_2O_3 NPs concentrations used in this study are 0, 10, 50, 250, and 500 µg/ml, and all the concentrations have demonstrated cytotoxic effects in concentration concentration-dependent manner. A significant decrease in cell number was observed in those cells treated with 250 and 500 µg/ml ($p < 0.0001$; $n \geq 3$). Cells treated with 50 and 10 µg/ml of Fe_2O_3 NPs did not show any significant changes in cell viability when compared with the control group ($p > 0.0001$; $n \geq 3$). Similarly, the same concentrations of the Fe_2O_3 NPs that are toxic to the cell were also applied to study their anti-proliferative potential and effect in a concentration-dependent manner, and a significant decrease in cell number was observed in those cells treated with 250 and 500 µg/ml ($p < 0.0001$; $n \geq 3$). In addition, 50 and 10 µg/ml of the synthesized NPs did not show any significant changes in cell viability compared with the control group ($p > 0.0001$; $n \geq 3$). Susanne et al. reported concentration-dependent cytotoxic and antiproliferative effects on MDA-MB 231 cells treated with Fe_2O_3 NPs, which also agrees with our findings [40]. Yusefi et al. revealed the cytotoxic potential of Fe_2O_3 NPs against A549, MCF7, HCT116 and HONE1, and the effect is also found to be concentration dependent as observed in our studies on MDA-MB 231 cells [27]. Phytochemicals present in plant extract play an essential role in the synthesis and stabilization of the NPs, and some of them have revealed their ability to inhibit transduction and metastasis in cancer cell lines [41, 42].

The cytotoxic potential revealed by our NPs might result from Fe^+ released from Fe_2O_3-NPs and its participation in the cell's metabolic activities [35]. Furthermore, the cytotoxic and anti-proliferative effect of zinc oxide NPs synthesized using plant extract revealed a strong effect on the viability of human breast cancer cells, which is found to be concentration-dependent [5].

MDA-MB 231 human breast cancer cells were treated with 50 and 10 µg/ml Fe_2O_3 NPs because they neither showed significant toxicity nor decreased the proliferation of the cells. Furthermore, 10 and 50 µg/ml synthesized Fe_2O_3 NPs showed an anti-migratory effect on MDA-MB 231 cells determined using wound healing assay (Figure 8). The motility index of MDA-MB 231 was drastically reduced with increased concentration of the synthesized NPs, as shown in figure 8, and 50 µg/ml revealed the lowest motility index when compared with the remaining Fe_2O_3-NPs concentrations. In addition, all Fe_2O_3-NPs concentrations revealed significant differences relative to the control ($p < 0.0001$; $n \geq 3$; Figure 8). Li et al. reported that fabricated Fe_3O_4 NPs capped with polydopamine

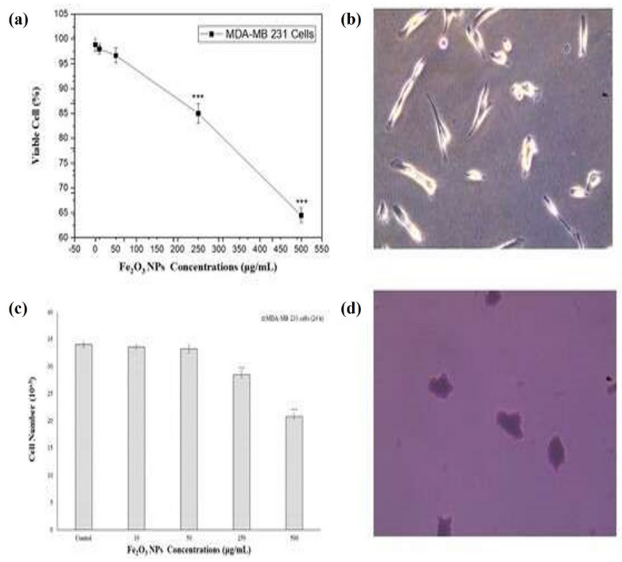

Figure 7: Effect of various concentrations of synthesized Fe_2O_3 NPs on the **(a)** Viability of MDA-MB 231 cells, **(b)** Typical phase-contrast light-microscopy image of the treated cells before adding tryphan blue, **(c)** Proliferation of MDA-MB 231 cells, and **(d)** Typical phase-contrast light-microscopy image of the treated cells obtained from tryphan blue exclusion assay.

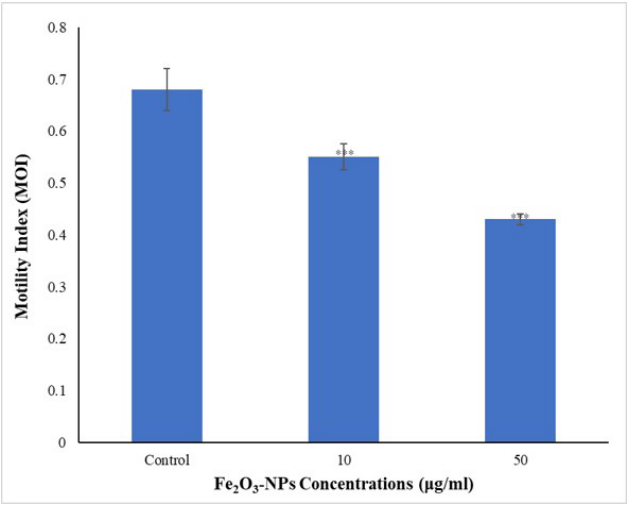

Figure 8. Anti-migratory effect of Fe_2O_3 NPs MDA-MB 231 cells.

promote mesenchymal stem cell migratory potential, which agrees with our findings [43]. Medicinal plants containing quercetin as an active ingredient showed anti-metastatic activity on strongly and weakly metastatic MatLYLu and AT-2 rat prostate cancer cell models, respectively [29, 43, 44].

Conclusion

Fe_2O_3 NPs were synthesized through a green route using *M. piperita* and characterized using UV-Vis, FTIR, XRD, SEM, and EDX analyses. The UV-Vis spectra of the synthesized NPs indicated an absorption peak at 302 nm, confirming both the successful synthesis and remarkable stability of the NPs. The synthesized NPs exhibited uniform spherical morphology and contained Fe, O, and N, indicating the successful synthesis of Fe_2O_3 NPs. Moreover, the Fe_2O_3 NPs synthesized through biosynthesis showed antimicrobial capabilities against *E. coli* and *B. cereus*. Additionally, the biosynthesized Fe_2O_3 NPs showed significant anti-migratory potential on MDA-MB 231 human breast cancer cells at lower concentrations, while higher concentrations revealed cytotoxic effects on the cells with an IC_{50} of 95.7 µg/ml. In summary, stable Fe_2O_3 NPs were synthesized using *M. piperita* aqueous extract, which demonstrated antimicrobial activity against *E. coli* and *B. cereus*, as well as cytotoxic, anti-proliferative and anti-migratory effects on highly metastatic human breast cancer cell lines.

Acknowledgements

None.

Conflict of Interest

The authors declare no conflict of interests.

Funding

Not applicable.

Ethical Approval

The use of cell lines was approved by the Ethical council of the university (Ethics approval number (BRCEC2011-01).

Data Availability

All the data are presented in the main manuscript.

References

1. Alphandéry E. 2020. Iron oxide nanoparticles for therapeutic applications. *Drug Discov Today* 25(1): 141-149. https://doi.org/10.1016/j.drudis.2019.09.020
2. Devatha CP, Thalla AK, Katte SY. 2016. Green synthesis of iron nanoparticles using different leaf extracts for treatment of domestic waste water. *J Clean Prod* 139: 1425-1435. https://doi.org/10.1016/j.jclepro.2016.09.019
3. Fazlzadeh M, Rahmani K, Zarei A, Abdoallahzadeh H, Nasiri F, et al. 2017. A novel green synthesis of zero valent iron nanoparticles (NZVI) using three plant extracts and their efficient application for removal of Cr(VI) from aqueous solutions. *Adv Powder Technol* 28(1): 122-130. https://doi.org/10.1016/j.apt.2016.09.003
4. Prabhakar R, Samadder SR. 2017. Aquatic and terrestrial weed mediated synthesis of iron nanoparticles for possible application in wastewater remediation. *J Clean Prod* 168: 1201-1210. https://doi.org/10.1016/j.jclepro.2017.09.063
5. Umar H, Kavaz D, Rizaner N. 2019. Biosynthesis of zinc oxide nanoparticles using *Albizia lebbeck* stem bark, and evaluation of its antimicrobial, antioxidant, and cytotoxic activities on human breast cancer cell lines. *Int J Nanomed* 14: 87-100. https://doi.org/10.2147/IJN.S186888
6. Gullu HH, Parlak M. 2016. Structural characteristics of thermally evaporated $Cu_{0.5}Ag_{0.5}InSe_2$ thin films. *Mater Res Express* 3(5): 055901. https://doi.org/10.1088/2053-1591/3/5/055901
7. Li XQ, Zhang WX. 2006. Iron nanoparticles: the core–shell structure and unique properties for Ni(II) sequestration. *Langmuir* 22(10): 4638-4642. https://doi.org/10.1021/la060057k
8. Morales-Morales JA. 2017. Synthesis of hematite a-Fe_2O_3 nano powders by the controlled precipitation method. *Ciencia Desarrollo* 8(1): 99-107. https://doi.org/10.19053/01217488.v8.n1.2017.4494

9. Chowdhury P, Roberts AM, Khan S, Hafeez BB, Chauhan SC, et al. 2017. Magnetic nanoformulations for prostate cancer. *Drug Discov Today* 22(8): 1233-1241. https://doi.org/10.1016/j.drudis.2017.04.018
10. El-Zahaby SA, Elnaggar YS, Abdallah OY. 2019. Reviewing two decades of nanomedicine implementations in targeted treatment and diagnosis of pancreatic cancer: an emphasis on state of art. *J Control Release* 293: 21-35. https://doi.org/10.1016/j.jconrel.2018.11.013
11. Suresh J, Pradheesh G, Alexramani V, Sundrarajan M, Hong SI. 2018. Green synthesis and characterization of zinc oxide nanoparticle using insulin plant (*Costus pictus* D. Don) and investigation of its antimicrobial as well as anticancer activities. *Adv Nat Sci Nanosci Nanotechnol* 9(1): 015008. https://doi.org/10.1088/2043-6254/aaa6f1
12. Kumar P, Tomar V, Kumar D, Joshi RK, Nemiwal M. 2022. Magnetically active iron oxide nanoparticles for catalysis of organic transformations: a review. *Tetrahedron* 106: 132641. https://doi.org/10.1016/j.tet.2022.132641
13. Zangeneh A, Zangeneh MM, Moradi R. 2020. Ethnomedicinal plant-extract-assisted green synthesis of iron nanoparticles using *Allium saralicum* extract, and their antioxidant, cytotoxicity, antibacterial, antifungal and cutaneous wound-healing activities. *Appl Organomet Chem* 34(1): e5247. https://doi.org/10.1002/aoc.5247
14. Dowlath MJH, Musthafa SA, Khalith SM, Varjani S, Karuppannan SK, et al. 2021. Comparison of characteristics and biocompatibility of green synthesized iron oxide nanoparticles with chemical synthesized nanoparticles. *Environ Res* 201: 111585. https://doi.org/10.1016/j.envres.2021.111585
15. Kharey P, Indoliya A, Gupta R, Poddar R, Sharma D, et al. 2022. Near-infrared active superparamagnetic iron oxide nanoparticles for magnetomotive optical coherence tomography imaging and magnetic hyperthermia therapeutic applications. *J Magn Magn Mater* 549: 169038. https://doi.org/10.1016/j.jmmm.2022.169038
16. Conde-Cid M, Paíga P, Moreira MM, Albergaria JT, Álvarez-Rodríguez E, et al. 2021. Sulfadiazine removal using green zero-valent iron nanoparticles: a low-cost and eco-friendly alternative technology for water remediation. *Environ Res* 198: 110451. https://doi.org/10.1016/j.envres.2020.110451
17. Khalil AF, Elkatry HO, El Mehairy HF. 2015. Protective effect of peppermint and parsley leaves oils against hepatotoxicity on experimental rats. *Ann Agric Sci* 60(2): 353-359. https://doi.org/10.1016/j.aoas.2015.11.004
18. Benabdallah A, Boumendjel M, Aissi O, Rahmoune C, Boussaid M, et al. 2018. Chemical composition, antioxidant activity and acetylcholinesterase inhibitory of wild *Mentha* species from northeastern Algeria. *South African J Botany* 116: 131-139. https://doi.org/10.1016/j.sajb.2018.03.002
19. Mahendran G, Rahman LU. 2020. Ethnomedicinal, phytochemical and pharmacological updates on Peppermint (*Mentha* × *piperita* L.)—a review. *Phytother Res* 34(9): 2088-2139. https://doi.org/10.1002/ptr.6664
20. Wei H, Kong S, Jayaraman V, Selvaraj D, Soundararajan P, et al. 2023. *Mentha arvensis* and *Mentha* × *piperita*-vital herbs with myriads of pharmaceutical benefits. *Horticulturae* 9(2): 224. https://doi.org/10.3390/horticulturae9020224
21. Tafrihi M, Imran M, Tufail T, Gondal TA, Caruso G, et al. 2021. The wonderful activities of the genus *Mentha*: not only antioxidant properties. *Molecules* 26(4): 1118. https://doi.org/10.3390/molecules26041118
22. Ćavar Zeljković S, Šišková J, Komzáková K, De Diego N, Kaffková K, et al. 2021. Phenolic compounds and biological activity of selected *Mentha* species. *Plants* 10(3): 550. https://doi.org/10.3390/plants10030550
23. Sivropoulou A, Kokkini S, Lanaras T, Arsenakis M. 1995. Antimicrobial activity of mint essential oils. *J Agric Food Chem* 43(9): 2384-2388. https://doi.org/10.1021/jf00057a013
24. Tsai ML, Wu CT, Lin TF, Lin WC, Huang YC, et al. 2013. Chemical composition and biological properties of essential oils of two mint species. *Tropical J Pharm Res* 12(4): 577-582. https://doi.org/10.4314/tjpr.v12i4.20
25. Beigi M, Torki-Harchegani M, Pirbalouti AG. 2018. Quantity and chemical composition of essential oil of peppermint (*Mentha* × *piperita* L.) leaves under different drying methods. *Int J Food Prop* 21(1): 267-276. https://doi.org/10.1080/10942912.2018.1453839
26. Brahmi F, Khodir M, Mohamed C, Pierre D. 2017. Chemical Composition and Biological Activities of Mentha Species. In El-Shemy HA (ed) Aromatic and Medicinal Plants-Back to Nature. IntechOpen, pp 47-79.
27. Yusefi M, Shameli K, Ali RR, Pang SW, Teow SY. 2020. Evaluating anticancer activity of plant-mediated synthesized iron oxide nanoparticles using *Punica granatum* fruit peel extract. *J Mol Struct* 1204: 127539. https://doi.org/10.1016/j.molstruc.2019.127539
28. Umar H, Kavaz D, Abubakar AL, Aliyu MR, Rizaner N. 2022. Synthesis of zinc oxide nanoparticles using *Ficus thonningii* aqueous extract and evaluation of its anti-oxidant and anti-microbial activities. *Bulgarian Chem Commun* 54(3): 277-282.
29. Umar H, Rizaner N, Usman AG, Aliyu MR, Adun H, et al. 2023. Prediction of cell migration in MDA-MB 231 and MCF-7 human breast cancer cells treated with *Albizia lebbeck* methanolic extract using multilinear regression and artificial intelligence-based models. *Pharmaceuticals* 16(6): 858. https://doi.org/10.3390/ph16060858
30. Kavaz D, Umar H, Shehu S. 2018. Synthesis, characterization, antimicrobial and antimetastatic activity of silver nanoparticles synthesized from *Ficus ingens* leaf. *Artif Cells Nanomed Biotechnol* 46(sup3): S1193-S1203. https://doi.org/10.1080/21691401.2018.1536060
31. Taffa DH, Hamm I, Dunkel C, Sinev I, Bahnemann D, et al. 2015. Electrochemical deposition of Fe_2O_3 in the presence of organic additives: a route to enhanced photoactivity. *RSC Adv* 5(125): 103512-103522. https://doi.org/10.1039/c5ra21290a
32. Mahdavi M, Namvar F, Ahmad MB, Mohamad R. 2013. Green biosynthesis and characterization of magnetic iron oxide (Fe_3O_4) nanoparticles using seaweed (*Sargassum muticum*) aqueous extract. *Molecules* 18(5): 5954-5964. https://doi.org/10.3390/molecules18055954
33. Saravanan A, Kumar PS, Varjani S, Karishma S, Jeevanantham S, et al. 2021. Effective removal of Cr(VI) ions from synthetic solution using mixed biomasses: kinetic, equilibrium and thermodynamic study. *J Water Process Eng* 40: 101905. https://doi.org/10.1016/j.jwpe.2020.101905
34. Saeed RA, Maqsood M, Saeed RA, Muzammil HS, Khan MI, et al. 2022. Plant-based foods and hepatocellular carcinoma: a review on mechanistic understanding. *Crit Rev Food Sci Nutr* 1-34. https://doi.org/10.1080/10408398.2022.2095974
35. Kiwumulo HF, Muwonge H, Ibingira C, Lubwama M, Kirabira JB, et al. 2022. Green synthesis and characterization of iron-oxide nanoparticles using *Moringa oleifera*: a potential protocol for use in low and middle income countries. *BMC Res Notes* 15(1): 1-8. https://doi.org/10.1186/s13104-022-06039-7
36. Singh N, Jenkins GJ, Asadi R, Doak SH. 2010. Potential toxicity of superparamagnetic iron oxide nanoparticles (SPION). *Nano Rev* 1(1): 5358. https://doi.org/10.3402/nano.v1i0.5358
37. Huber DL. 2005. Synthesis, properties, and applications of iron nanoparticles. *Small* 1(5): 482-501. https://doi.org/10.1002/smll.200500006
38. Batool F, Iqbal MS, Khan SUD, Khan J, Ahmed B, et al. 2021. Biologically synthesized iron nanoparticles (FeNPs) from *Phoenix dactylifera* have anti-bacterial activities. *Sci Rep* 11(1): 22132. https://doi.org/10.1038/s41598-021-01374-4
39. Attia NF, Abd El-Monaem EM, El-Aqapa HG, Elashery SE, Eltaweil AS, et al. 2022. Iron oxide nanoparticles and their pharmaceutical applications. *Appl Surf Sci Adv* 11: 100284. https://doi.org/10.1016/j.apsadv.2022.100284
40. Irshad R, Tahir K, Li B, Ahmad A, Siddiqui AR, et al. 2017. Antibacterial activity of biochemically capped iron oxide nanoparticles: a view towards green chemistry. *J Photochem Photobiol B Biol* 170: 241-246. https://doi.org/10.1016/j.jphotobiol.2017.04.020

41. Kossatz S, Grandke J, Couleaud P, Latorre A, Aires A, et al. 2015. Efficient treatment of breast cancer xenografts with multifunctionalized iron oxide nanoparticles combining magnetic hyperthermia and anti-cancer drug delivery. *Breast Cancer Res* 17: 1-17. https://doi.org/10.1186/s13058-015-0576-1

42. Gumushan-Aktas H, Altun S. 2016. Effects of *Hedera helix* L. extracts on rat prostate cancer cell proliferation and motility. *Oncol Lett* 12(4): 2985-2991. https://doi.org/10.3892/ol.2016.4941

43. Li X, Wei Z, Lv H, Wu L, Cui Y, et al. 2019. Iron oxide nanoparticles promote the migration of mesenchymal stem cells to injury sites. *Int J Nanomed* 14: 573-589. https://doi.org/10.2147/IJN.S184920

44. Priya, Naveen, Kaur K, Sidhu AK. 2021. Green synthesis: an eco-friendly route for the synthesis of iron oxide nanoparticles. *Front Nanotechnol* 3: 655062. https://doi.org/10.3389/fnano.2021.655062